

PAPER • OPEN ACCESS

A generalized saturated capacitor model for hysteresis in piezoelectric materials

To cite this article: Y Liu *et al* 2019 *IOP Conf. Ser.: Mater. Sci. Eng.* **474** 012004

View the [article online](#) for updates and enhancements.

A generalized saturated capacitor model for hysteresis in piezoelectric materials

Y Liu*, M Huo and M Tang

Department of Aerospace Engineering, Harbin Institute of Technology, Harbin, 150001, China

*E-mail: liu-yanfang@hotmail.com

Abstract. A generalized saturated capacitor (GSC) model is proposed for hysteresis in piezoelectric materials. It introduces the Weiss domains (WDs) with a negative capacitance switch (NCS) into the saturated capacitor model. The WD with NCS is modeled as a parallel network of a charge-limited capacitor and perfect one. It is further made equivalent to a series network of a voltage-limited capacitor (VLC) with negative elastance values and a perfect capacitor, which induces the GSC model to become a series network of several VLCs with positive or negative elastances. The GSC model can capture non-convex hysteresis loops and is self-invertible, namely the inverse GSC model has the same structure as the original (forward) one but differs by its parameters. The proposed model effectiveness is corroborated by the experimental data, with the maximal discrepancy not exceeding 1%.

1. Introduction

Piezoelectric materials are characterized by many advantages such as fast response and high stiffness. They are widely used as sensors or actuators in many applications such as nano-manipulation, active vibration control, and nano-positioning [1]. However, the unwanted hysteresis limits their performance. It can lead to errors up to 15% of the full range of a piezoelectric actuator (PEA) or even instability of the system [1, 2].

Modeling and compensating for hysteresis is reliable and straightforward. Thus, it becomes one of the most popular approaches to handle it [3, 4]. The hysteresis is described by models such as the Preisach model [5, 6], Prandtl-Ishlinskii model [7-11], and Bouc-Wen model [12, 13]. Then, the corresponding inverse model is constructed and connected in series with a PEA to eliminate hysteresis [9, 14]. Unfortunately, these models are a purely mathematical description of the observed hysteresis phenomenon and provide little physical interpretation. Hence, they hardly give any insight into the generation mechanism of the hysteresis.

A hysteresis model that is based on the physical principle is formulated by James C. Maxwell [15]. Its electric interpretation is referred to as the saturated capacitor (SC) model [16, 17]. The SC model represents the Weiss domain (WD) by a series network of a voltage-limited capacitor (VLC) and a perfect capacitor. Since a PEA contains many WDs, it is modeled by a series network of several VLCs. Unfortunately, as the SC model only considers WDs with positive capacitance switch (PCS), it can just capture convex hysteresis loops. A modified model that is capable of capturing non-convex hysteresis is proposed in [18]. However, it is too complicated to generate the inverse model.

In this paper, the WD with a negative capacitance switch (NCS) is introduced into the SC model. The WD with NCS is modeled by a parallel network of a charge-limited capacitor (CLC) and a perfect



capacitor, which is further approximated by a serial network of a VLC with negative elastance and a perfect capacitor. Then a generalized SC (GSC) model is constructed, which has the same structure as the SC model but allows some VLCs to have negative elastances. If a GSC model is connected in series with a PEA, it can pre-shape the control input of the PEA and generate the inverse hysteresis to compensate for the nonlinearity.

2. Modeling and identification of hysteresis in PEAs

2.1. Saturated capacitor model

A PEA consists of many WDs, each of which has the same dipole orientation. When an electric field is applied to a WD, it performs like a capacitor. However, its capacitance is not constant. Without loss of generality, the continuous change of capacitance is simplified to be a switch between two constants.

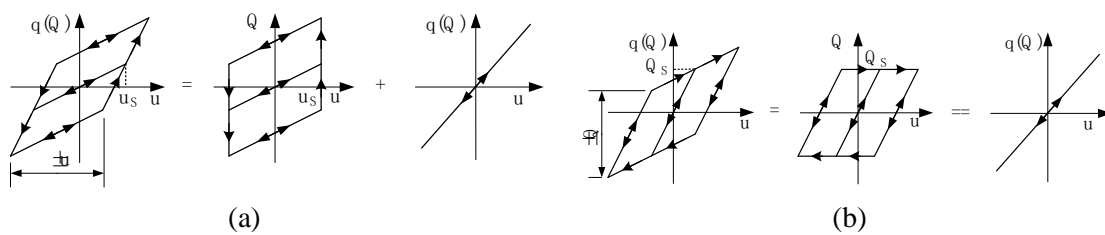


Figure 1. Charge-voltage property for a WD with (a) PCS and (b) NCS. Symbol u is the excitation voltage of the WD. Symbols Q and q are, respectively, the charges applied to and stored in the WD. Symbols u_s and Q_s represent the saturation voltage and the saturation charge, respectively. Symbols δu and δQ represent the changes of the applied voltage and charge, respectively. Symbols $+$ and $//$ represent series connection and parallel connection, respectively.

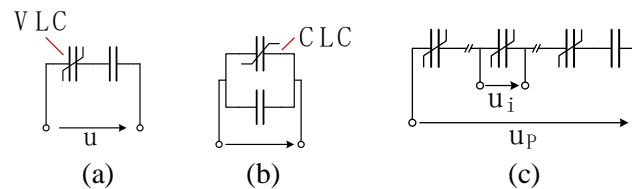


Figure 2. Equivalent circuits for a WD with (a) PCS, (b) NCS, and (c) for the SC model.

The charge-voltage property of a WD with PCS [16, 17] is shown in figure 1(a). The increase/decrease of the applied voltage δu has a threshold value. Before δu reaches this value, the WD performs like a perfect capacitor, namely the change rate of the charges stored and applied to it, i.e. \dot{q} , and \dot{Q} , are proportional to the change rate of the voltage applied to it, i.e., \dot{u} . Once the increase/decrease of the voltage reaches the threshold value, the capacitance switches to a more significant value. The capacitance always turns back to the smaller value if the change of the voltage switches direction. The WD with PCS can be equivalent to a series network of a VLC and a perfect capacitor, as shown in figure 2(a). The charge-voltage property of a VLC is also given in figure 1(a). The voltage across a VLC has a saturation value u_s . If \dot{Q} does not change direction and u does not reach u_s , $\dot{q} = \dot{Q} = \dot{u} / S$. Once u_s is reached, charges cross the VLC without any resistance thus $u = u_s$ and $Q = Q_s$. Thus, the VLC is governed by

$$\dot{q} = \begin{cases} \dot{Q} & |q| < Q_s \\ 0 & |q| \geq Q_s \end{cases} \quad (1)$$

$$u = Sq \quad (2)$$

where S is the elastance (i.e., the inverse of capacitance) and $S \in \mathbb{R}^+$.

Insofar as PEA consists of many WDs, the SC model represents it by a series network of several VLCs and one ideal capacitor, as shown in figure 2(c). Herein, the ideal capacitor is equivalent to the series network of ideal capacitors of all the WDs. It can be seen as a VLC with infinite saturation charge. Meanwhile, it can avoid computation singularity in the simulation—the charge becomes infinite if the voltage increases slightly after all the VLCs are saturated, which leads to singularity in the simulation. Then, the governing equation of the SC model is

$$\dot{q}_i = \begin{cases} \dot{Q} & |q_i| < Q_{s,i} \\ 0 & |q_i| \geq Q_{s,i} \end{cases} \quad (3)$$

$$u_p = \sum_{i=1}^n S_i q_i \quad (4)$$

Its discrete form is

$$q_{i,k+1} = \begin{cases} \hat{q}_{i,k+1} & |\hat{q}_{i,k+1}| < Q_{s,i} \\ Q_{s,i} \text{sign} \hat{q}_{i,k+1} & |\hat{q}_{i,k+1}| \geq Q_{s,i} \end{cases} \quad (5)$$

$$\hat{q}_{i,k+1} = u_{i,k} + Q_{k+1} - Q_k \quad (6)$$

$$u_{p,k+1} = \sum_{i=1}^n S_i q_{i,k+1} \quad (7)$$

where i and k are the serial numbers of VLCs and samples, respectively. Equation (5) is the state equation and updates q_i . Equation (6) calculates virtual states \hat{q}_i . Equation (7) gives the output voltage u_p .

As this model considers WDs with PCS only, it can hardly describe the non-convex hysteresis. Some WDs may have NCS. In the next subsection, the SC model is generalized by introducing WDs with NCS.

2.2. Generalized saturated capacitor model

The charge-voltage property of a WD with NCS is shown in figure 1(b). The increase/decrease of the applied charge δQ has a threshold value Q_s . Before δQ reaches this value, q and Q are proportional to u . The capacitance becomes smaller once δQ reaches Q_s . The capacitance always switches back to the more significant value if the change of u switches its direction to the opposite one. The WD with NCS can be represented by a parallel network of a CLC and a perfect capacitor, as shown in figure 1(b). The charge-voltage property of a CLC is also given in figure 2(b). The charge applied to a CLC has a saturation value Q_s . Before Q reaches to Q_s or the change of u switches direction, $\dot{q} = \dot{Q} = C\dot{u}$. The CLC has similar behavior as a perfect insulator once Q reaches Q_s , namely, charges cannot cross the CLC and $q = Q = Q_s$. Its governing equation is

$$\dot{Q} = \begin{cases} C\dot{u} & |Q| < Q_s \\ 0 & |Q| \geq Q_s \end{cases} \quad (8)$$

where C is the capacitance.

Considering WDs with NCS, the equivalent circuit of a PEA becomes quite complex. Fortunately, the parallel network of a CLC and a perfect capacitor can be represented by a series network of a VLC and a perfect capacitor. Let

$$C_1 + C_c = \frac{C_v C_1}{C_v + C_1} \quad (9)$$

where C_1 , C_c , and C_v are capacitances of the ideal capacitor, CLC, and VLC, respectively. Then

$$C_v = -\frac{C_1^2}{C_c} - C_1 \quad (10)$$

Since C_1 and C_c are positive, then C_v is negative. Thus, equation (10) indicates that a WD with NCS can be represented by a WD with PCS. However, the elastance $S = 1/C \in \mathbb{R}^-$. Thus, the GSC can be represented by the circuit given in figure 2(c) and the formula in equation (3).

2.3. Parameters' identification

The initial parameters can be calculated from the initial ascending curve [16, 17] or the major ascending/descending curve. The main points are separating the curve into n segments, calculating the average slope of each segment, and then obtaining $Q_{s,i}$ and S_i . Further, the parameters are optimized by solving the minimization problem

$$\min_{\substack{S_1, \dots, S_n \\ Q_{s,1}, \dots, Q_{s,n}}} \sqrt{\frac{1}{N} \sum_{k=1}^N [Q(t_k) - \text{GSC}[u](t_k)]^2} \quad (11)$$

where GSC denotes the GSC model operator and N is the number of samples. For simplification, $Q_{s,i}$ is treated as fixed, i.e., evenly distributed in the desired range, and only S_i are optimized as follows

$$\min_{S_1, \dots, S_n} \sqrt{\frac{1}{N} \sum_{k=1}^N [Q(t_k) - \text{GSC}[u](t_k)]^2} \quad (12)$$

3. Properties of the GSC model and experimental validation

According to the above analysis, the generalization of the SC model is quite simple by replacing the constraint $S_i \in \mathbb{R}^+$ by $S_i \in \mathbb{R}$. However, this simple replacement yields some remarkable properties, namely (i) self-invertible property and (ii) non-convex hysteresis property.

3.1. Self-invertible property

Property 1 (Self-invertible property). The GSC model is self-invertible, which means that the inverse of a GSC model has the same structure as the GSC model but with different parameters.

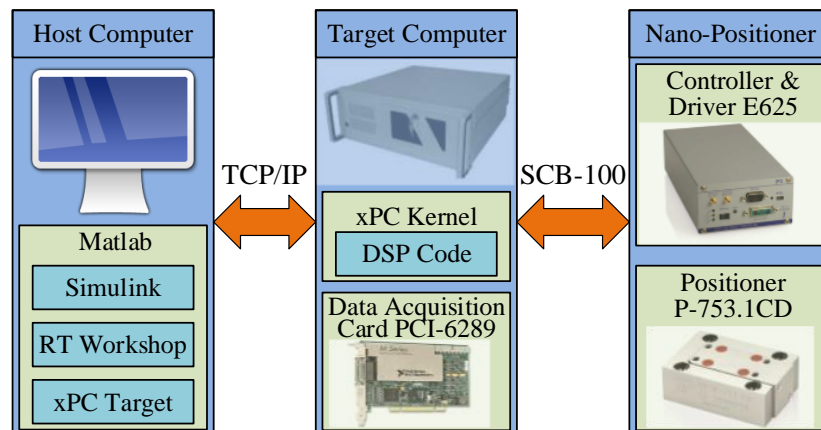


Figure 3. Experiment setup of the PEA-based nanopositioning system.

A PEA-based nano-positioning system is shown in figure 3. It is employed to collect data to demonstrate the self-invertible property. This system consists of a positioner P-753.1CD integrated with a capacitive sensor, a target computer equipped with a data acquisition card PCI-6289, and a host computer working under Matlab environment.

As shown in figure 4(a), in identifying the forward GSC model, the normalized input and output of the nanopositioning system are served as the input and output of the model, respectively. However, in identifying the inverse GSC model, the input and output are inverted, as shown in figure (b). The initial ascending curve is used to calculate the initial parameters, and the major hysteresis loop is used to optimize these parameters. Then the experiment system is excited by the triangle signal with decreasing amplitudes. The output displacement and the input voltage are collected and normalized. The normalized input u is applied to the identified forward GSC model and generated the model output y_F . Then, y_F is applied to the identified inverse GSC model and produced the model output u_1 .

The parameters for the forward and the inverse models are given in table 1. As shown in figure 5, the hysteresis loops generated from the forward model are quite similar to that is obtained from the

experiment system. These hysteresis loops are all counterclockwise. The area of the hysteresis loop represents the energy consumption of the nonlinearity. The normalized root mean square (NRMS) error is 0.58%, which demonstrates that the GSC model can capture the hysteresis loop directly and efficiently. The hysteresis loops generated from the inverse model are clockwise. They are symmetrical with the hysteresis loops that are generated from the forward model about the line $y = u$. The NRMS error is 0.26%, which illustrates that the GSC model is capable of describing the inverse hysteresis efficiently, too. From u to u_1 , signals pass through the forward model and the inverse model. In other words, the inverse model is compensated by the forward model. The curve $u - u_1$ shown in figure (d) represents the compensation results. The uncompensated error is 0.26%, which verifies that the forward model can linearize the inverse model effectively.

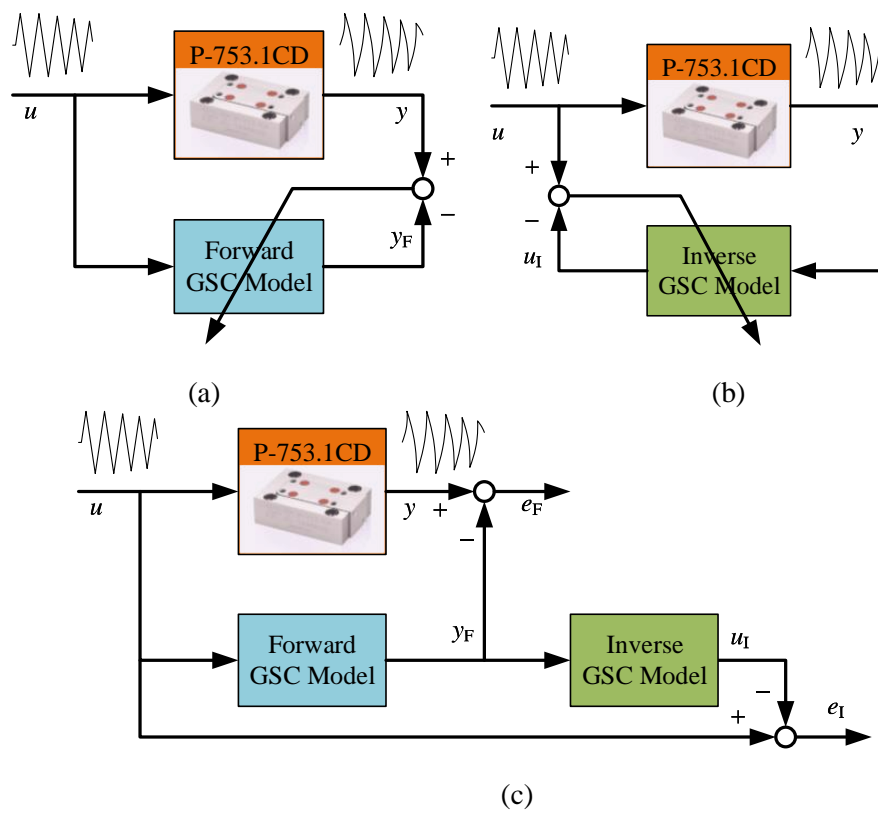


Figure 4. Identification of (a) the forward GSC model and (b) the inverse GSC mode and (c) model evaluation. Symbols u and y represent the normalized input voltage and output displacement of the experiment system. Symbol y_F represents the output of the forward GSC model. Symbol u_1 represents the output of the inverse GSC model. Symbols e_F and e_I represent the modeling errors of the forward and the inverse GSC model, respectively.

Table 1. Identified parameters of the forward and the inverse GSC models.

Model	S_1	S_2	S_3	S_4	S_5
Forward GSC model	-0.1484	-0.1056	-0.0816	-0.0714	1.1628
Inverse GSC model	0.2448	0.1083	0.0586	0.0560	0.8544

If $S \in \mathbb{R}^+$, the ascending curve is convex. However, as shown in figure 5(a), the experimental ascending curves are concave. Thus, the original SC model can hardly capture the forward hysteresis

loops. It is an inverse hysteresis model. The GSC model can forward-capture the hysteresis loops by utilizing negative elastances, which is also indicated by the identified parameters in Table 1.

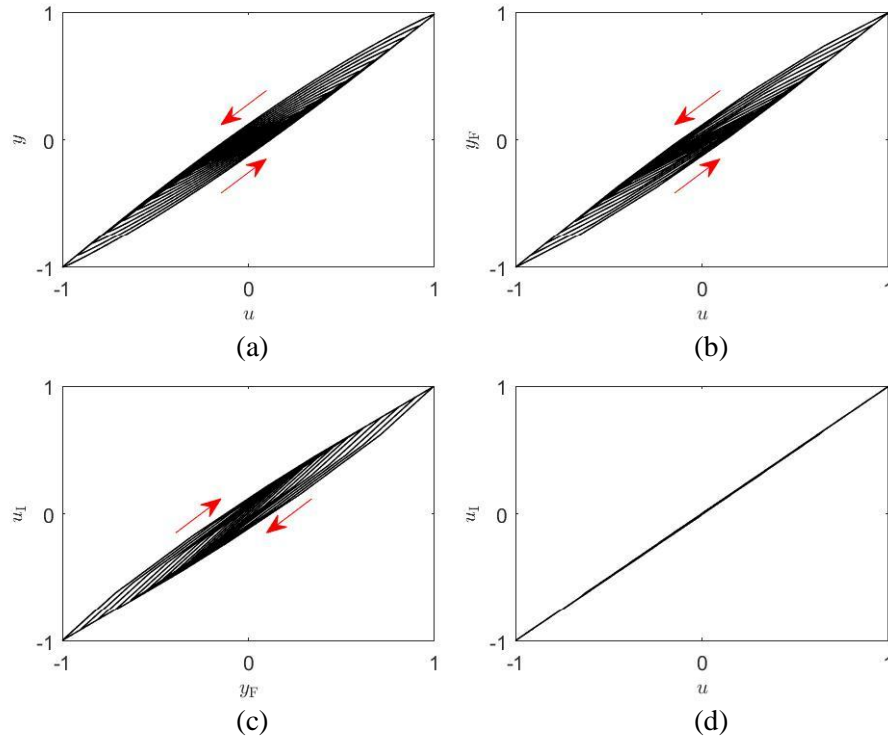


Figure 5. Hysteresis nonlinearities: (a) experiment, (b) forward model, and (c) inverse model and (d) compensated results.

3.2. Non-convex hysteresis property

Actually, in the above subsection, it has been demonstrated that the GSC model is capable of describing concave ascending curves. However, it is not sufficient to prove that the GSC model can define the non-convex hysteresis loops. In this subsection, experimental data will be employed to show that the GSC's capability of modeling the non-convex loops.

Property 2 (Non-convex hysteresis property). The GSC model is capable of generating non-convex hysteresis loops.

Table 2. Parameters of the GSC model for non-convex hysteresis loops.

i	S_i	i	S_i	i	S_i	i	S_i	i	S_i
1	-0.0688	4	-0.3334	7	0.4400	10	2.4334	13	0.1425
2	-0.1612	5	0.3420	8	-1.6728	11	2.4938	14	0.2370
3	0.2496	6	-0.5462	9	-4.3660	12	0.6859	15	0.1693

The data provided in [19] are depicted in figure 6(a). The experimental hysteresis loops are non-convex. The identified parameters are given in table 2. It is seen from the table that, to capture the concave part of the hysteresis loop, some VLCs have negative elastances. With these parameters, the hysteresis loops generated from the GSC model are also presented in figure 6(a). They follow the experimental ones closely. As seen in figure 6(b), the maximum error is at the position where the curve $u - y$ intersects the u axis and is less than 5%. The NRMS error is about 0.94%. The $u - y$ curve has a large slope when it crosses $y = 0$ the axis. Thus, for this position, more VLCs are needed to capture the

change of the slope. In other words, an even distribution of $Q_{s,i}$ is not quite reasonable. Properly distributing $Q_{s,i}$ or increasing the number of VLCs may reduce the modeling error. On the other hand, instead of a piecewise linear function, employing a continuous function to capture the slope change of the ascending curves may also obtain improved performances. These efforts will be made in future studies.

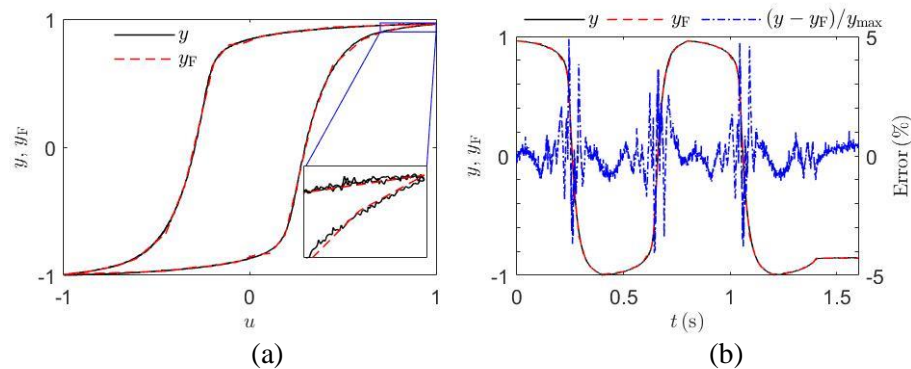


Figure 6. Performance of GSC model on modeling the non-convex hysteresis: (a) the hysteresis loops generated from experiment and model, i.e., u - y and u - y_F , and (b) modeling errors.

4. Conclusions

This paper proposes a generalized saturated capacitor (GSC) model for the hysteresis in piezoelectric materials. It introduces the Weiss domains (WDs) with negative capacitance switch (NCS) into the saturated capacitor model. The WD with NCS is represented by a parallel network of a charge-limited capacitor and a perfect capacitor and further described by a series network of a voltage-limited capacitor (VLC) with negative elastance and a perfect capacitor. Then, a piezoelectric actuator is modeled as a series network of several VLCs, which can have positive or negative elastances. The GSC model is capable of describing non-convex hysteresis and is self-invertible. Its effectiveness and self-invertible property are verified experimentally. Results show that the modeling error is less than 1% for both forward and inverse models. The maximum error occurs at the position where the hysteresis loop has a sharp slope. Increasing the number of VLCs distributed at this position may reduce the modeling error. Employing a continuous function to describe the hysteresis loop may also improve the model performance.

Acknowledgment

The authors express their gratitude to Prof. Christopher S. Lynch of the University of California for kindly providing the experimental data [19]. This work is partially supported by National Natural Science Foundation of China (11672093, 51705109, and U1737207), Special Foundation of Heilongjiang Postdoctoral Science (LBHTZ1609), the Innovation Fund of the Shanghai Academy of Spaceflight Technology under Grant SAST-2018-109, and Fundamental Research Funds for the Central Universities of China (HIT.NSRIF.201622).

References

- [1] Devasia S, Eleftheriou E and Moheimani S R 2007 *IEEE Trans Control Syst. Technol* **15** 802-23
- [2] Aguirre G, Janssens T, van Brussel H and Al-Bendera F 2012 *Mech Syst Signal Proc* **b** 218-31
- [3] Wang Z, Zhang Z and Mao J 2012 *Electron Lett* **48** 1459-60
- [4] Liu L, Tan K K, Chen S, Teo C S and Lee T H 2013 *IEEE Trans Indust Inform* **9** 859-68
- [5] Zhang J, Merced E, Sepúlveda N and Tan X 2014 *IEEE-ASME Trans Mechatron* **19** 579-88
- [6] Mackenzie I and Trumper D L 2016 *IEEE-ASME Trans. Mechatron* **21** 4-16
- [7] Sun Z, Song B, Xi N, Yang R, Hao L, Yang Y and Chen L 2017 *IEEE Trans Ind Inform* **64** 5513-

23

- [8] Chen X, Su C, Li Z and Yang F 2016 *IEEE Trans Ind Inform* **63** 6471-81
- [9] Gu G, Zhu L and Su C 2014 *IEEE Trans Ind Inform* **61** 1583-95
- [10] Li Z and Shan J 2017 *IEEE-ASME Trans Mechatron* **22** 1903-13
- [11] Li Z and Shan J 2017 *IEEE Trans Ind Inform* **64** 8588-97
- [12] Aschemann H and Schindele D 2014 *IEEE Trans Ind Inform* **61** 3620-29
- [13] Xu Q 2013 *IEEE Trans Ind Inform* **60** 3927-37
- [14] Janaideh M A and Krejčí P 2013 *IEEE-ASME Trans Mechatron* **18** 1498-507
- [15] Goldfarb M and Celanovic N 1997 *IEEE Contr Syst* **17** 69-79
- [16] Liu Y, Shan J, Gabbert U and Qi N 2013 *Smart Mater Struct* **22** 5020
- [17] Liu Y, Liu H, Wu H and Dan Z 2016 *Electron Lett* **52** 188-90
- [18] Liu Y, Shan J, Meng Y and Zhu D 2016 *IEEE-ASME T Mech* **21** 38-43
- [19] Rauls M B, Dong W, Huber J E and Lynch C L 2011 *Acta Mater* **59** 2713-22